Assimilation of Radar Radial Velocity Data with the WRF Ensemble-3DVAR Hybrid System for the Prediction of Hurricane Ike (2008)

Yongzuo Li, Xuguang Wang, and Ming Xue

School of Meteorology and Center for Analysis and Prediction of Storms
University of Oklahoma, Norman, Oklahoma 73072

January, 2012

Submitted to Monthly Weather Review

Corresponding author address:
Yongzuo Li
Center for Analysis and Prediction of Storms
University of Oklahoma,
120 David L. Boren Blvd, Norman OK 73072
yongzuo.li@ou.edu

Abstract

An enhanced version of the hybrid ensemble-3DVAR data assimilation system for the WRF model is applied to the assimilation of radial velocity (Vr) data from two coastal WSR-88D radars for the prediction of Hurricane Ike (2008) before and during its landfall. In this hybrid system, flow-dependent ensemble covariance is incorporated into the varitional cost function using the extended control variable method. The analysis ensemble is generated by updating each forecast ensemble member with perturbed radar observations using the hybrid scheme itself. The Vr data are assimilated every 30 minutes for 3 hours immediately after Ike entered the coverage of the two coastal radars.

The hybrid method produces temperature increments showing rainband structures and positive increments in the vortex core region, and a warm core throughout the hurricane depth in the final analysis. In contrast, the 3DVAR produces much weaker and smoother increments with negative values at the vortex center at lower levels. Wind forecasts from the hybrid analyses fit the observed radial velocity better than that from 3DVAR, and the 3-h accumulated precipitation forecasts from the hybrid are also more skillful. The track forecast is slightly improved by the hybrid method and slightly degraded by the 3DVAR compared to the forecast from the GFS analysis. All experiments assimilating the radar data show much improved intensity analyses and forecasts compared to the experiment without assimilating radar data. The better forecast of the hybrid indicates that the hybrid method produces dynamically more consistent state estimations. Little benefit of including the tuned static component of background error covariance in the hybrid is found.

1. Introduction

Tropical cyclones (TCs) are among the most costly forms of natural disaster (Pielke et al. 2008). An accurate TC forecast will require not only a numerical model to realistically simulate both the TC itself and its environment, but also a data assimilation (DA) system that can effectively use the observations to accurately estimate the initial TC vortex and the environment where the TC is embedded in.

To address the TC initialization issue, many previous studies adopted the vortex relocation and/or bogussing (e.g., Liu et al. 2000; Kurihara et al. 1995; Zou and Xiao 2000) techniques. While such techniques are non-trivial and have been shown to improve the hurricane forecast, how to maintain the dynamical and thermo-dynamical coherency of the hurricane and its environment is probably the biggest challenge with such methods.

Recently, several studies have explored the use of ensemble-based DA methods to initialize hurricane forecasts and have shown great promise (e.g., Torn and Hakim 2009; Zhang et al. 2009; Li and Liu 2009; Hamill et al. 2011; Wang 2011; Dong and Xue 2011). The key with ensemble-based DA is the use of an ensemble to estimate the forecast error statistics in a flow-dependent manner. Therefore, the observation information will be properly weighted and spread consistent with the background hurricane forecasts; and perhaps more importantly, the ensemble covariance can realistically infer the flow-dependent cross-variable error statistics and therefore update state variables not directly observed in a dynamically and thermodynamically consistent manner.

One candidate in ensemble-based DA is the hybrid ensemble-variational DA method. It has been proposed (e.g., Hamill and Snyder 2000; Lorenc 2003; Etherton and Bishop 2004; Zupanski 2005; Wang et al. 2007b, 2008a; Wang 2010), implemented and tested with real numerical weather prediction (NWP) models and real data recently (e.g., Buehner 2005; Wang et al. 2008b; Buehner et al. 2010ab; Wang 2011; Wang et al. 2011; Whitaker et al. 2011; Kleist et al. 2011). Compared to a standard variational method (VAR) that typically uses static background error covariance, ensemble covariance is incorporated into the VAR framework to provide a flow-dependent estimate of the background error covariance and the ensemble can be generated by a version of the ensemble Kalman filter (EnKF). Recent studies have suggested that the hybrid DA systems may represent the "best of both worlds" by combining the best aspects of the variational and EnKF systems (e.g., Wang et al. 2007a, 2008ab, 2009; Zhang et al. 2009; Buehner et al. 2010ab; Wang 2010). While preliminary tests of the hybrid DA system with real NWP models and data have shown great potential of the method for non-TC forecasts (e.g., Wang et al. 2008b; Buehner et al. 2010ab) and for forecasts of TC tracks (e.g., Wang 2011; Whitaker et al. 2011), to the author's best knowledge, to date there is no published study applying hybrid DA method to the assimilation of radar data at a convection-allowing resolution for TC predictions. This study serves as a pilot study applying the hybrid ensemble-3DVAR system developed for the WRF model (Wang et al. 2008a) to explore its potential for assimilating radar observation for hurricane forecasts. As a first step of such study, we focus on assimilating radar radial velocity data.

More specifically, this study applies and explores the WRF ensemble-3DVAR hybrid system to the assimilation of coastal WSR-88D radar radial velocity data for the prediction of Hurricane Ike (2008) (Fig. 1). Ike is the third most destructive landfalling hurricane in the recorded history of United States. Previous studies (e.g., Zhao and Xue 2009) have shown significant impact of the radar data for this case using ARPS 3DVAR/cloud analysis package. The remainder of this paper is organized as follows: Section 2 presents the methodology and section 3 discusses the experiment design. The experiment results are discussed in Section 4 while the final section summarizes the main conclusions of this study.

2. Methodology

a. The hybrid ensemble-3DVAR scheme

A diagram of the hybrid DA system is shown in Fig. 2. Similar to Hamill and Snyder (2000), the following four steps are repeated for each DA cycle: 1. Perform K (K is the ensemble size) number of ensemble forecasts to generate background forecast fields at the time of analysis; 2. Calculate ensemble forecast perturbations to be used by the hybrid cost function for flow-dependent covariance by subtracting ensemble mean from each member; 3. Generate K independent sets of perturbed observations by adding random perturbations to the observations; 4. Obtain the analysis increment for each ensemble member through minimization of the hybrid cost function using one set of perturbed observations. Steps 1 through 4 are repeated for each of the follow-on cycles, with the ensemble analyses providing initial conditions for step 1. In step 3, the random perturbations added to the observations are drawn from a Gaussian distribution with a mean of zero and a standard deviation of the observation error. This is analogous to the 'perturbed observation method' employed in the classic ensemble Kalman filter (Evensen 2003). In the original work of Wang et al. (2008a) testing the hybrid WRF DA system, the ensemble transform Kalman filter (ETKF) was used to update forecast perturbations.

A brief review on the extended control variable method for incorporating ensemble covariance into a WRF 3DVAR framework is given here. For detailed discussions, readers are referred to Wang et al. (2007b, 2008a).

For state vector $\mathbf{x}$, the analysis increment of the hybrid scheme, $\mathbf{x}'$, is the sum of two terms,

$$\mathbf{x}' = \mathbf{x}_1' + \sum_{k=1}^{K} \left(\mathbf{a}_k \circ \mathbf{x}_k^e \right). \tag{1}$$

The first term $\mathbf{x}_1'$ in Eq. (1) is the increment associated with WRF 3DVAR static background covariance and the second term is the increment associated with flow-dependent covariance. Here, $\mathbf{a}_k$ is the extended control variable as defined by Lorenc (2003), $\mathbf{x}_k^e$ is the k^{th} ensemble perturbation state vector. The symbol 'o' denotes the Schur product (element by element product) of the vectors $\mathbf{a}_k$ and $\mathbf{x}_k^e$.

The cost function for WRF ensemble-3DVAR hybrid is

$$J(\mathbf{x}_1', \mathbf{a}) = \beta_1 J_b + \beta_2 J_e + J_o,$$

$$= \beta_1 \frac{1}{2}(\mathbf{x}_1')^T \mathbf{B}^{-1}(\mathbf{x}_1') + \beta_2 \frac{1}{2}(\mathbf{a})^T \mathbf{A}^{-1}(\mathbf{a}) + \frac{1}{2}(\mathbf{y}^{o'} - \mathbf{H}\mathbf{x}')^T \mathbf{R}^{-1}(\mathbf{y}^{o'} - \mathbf{H}\mathbf{x}'). \tag{2}$$

J_b is the traditional WRF 3DVAR background term associated with the static covariance $\mathbf{B}$ and J_e is the hybrid term associated with flow-dependent covariance. $\mathbf{a}$ is defined as $\mathbf{a}^{\mathrm{T}} = (\mathbf{a}_1^{\mathrm{T}}, \mathbf{a}_2^{\mathrm{T}}, \cdots, \mathbf{a}_{\mathrm{K}}^{\mathrm{T}})$. J_o is the observation term associated with observation error covariance $\mathbf{R}$. The innovation vector $\mathbf{y}^{o\prime}$ is defined as, $\mathbf{y}^{o\prime} = \mathbf{y}^o - \mathbf{H}(\mathbf{x}^b)$, where $\mathbf{y}^o$ is the observation vector, $\mathbf{x}^b$ is the background forecast state vector, and $\mathbf{H}$ is the linearized observation operator.

The weights of the static covariance and flow-dependent covariance are determined by factors β_1 and β_2 according to relationship

$$\frac{1}{\beta_1} + \frac{1}{\beta_2} = 1, \tag{3}$$

which conserves the total variance.

As described in Wang et al. (2008a), the ensemble covariance localization, denoted as $\mathbf{A}$, has horizontal and vertical components. In this study, both the horizontal and vertical localization are applied. Specifically, the horizontal localization is modeled by a recursive filter transform as in Wang et al. 2008a. The vertical localization is implemented by transforming the extended control variable **a** in Eq. (2) with empirical orthogonal functions (EOFs). The correlation matrix, denoted as Cov, from which the EOFs is derived, follows

$$\mathrm{Cov}(k_1,k_2)=\exp\left(-\frac{d^2}{L^2}\right), \tag{4}$$

where d is the distance between model levels k_1 and k_2 and L is the vertical localization radius. Existing EOF codes in the WRF 3DVAR for modeling the vertical static error covariance is used for the vertical ensemble covariance localization purpose.

3. Experimental design

a. The WRF model configuration

The Advanced Research WRF (ARW) model version 3 is used in this study (Skamarock et al. 2008). The model is compressible, three-dimensional, non-hydrostatic, discretized on a Arakawa C grid with terrain-following mass-based sigma coordinate levels. In this study, the WRF model is configured with 401x401 horizontal grid points at 5-km grid spacing (Fig. 1), and 41 vertical levels with the model top at 100 hPa. The WRF single-moment six-class scheme (Hong et al. 2004) is chosen for the explicit microphysics processes. Since the grid resolution may not fully resolve the hurricane convective features, the Grell-Devenyi cumulus parameterization scheme (Grell; Devenyi 2002) is included. Other physics parameterizations schemes used include the Yonsei University (YSU) (Noh et al. 2003) scheme for planetary boundary layer parameterization, the 5-layer thermal diffusion model for land surface processes (Skamarock et al. 2008), the Rapid Radiative Transfer Model (RRTM) longwave (Mlawer et al. 1997), and the MM5 shortwave (Dudhia 1989) radiation parameterization.

b. The radar data processing

The radial velocity data from coastal WSR-88D radars at Houston, Texas (KHGX) and Lake Charles, Louisianan (KLCH) are processed using a modified version of the Four Dimensional Dealiasing Algorithm (James; Houze 2001). The algorithm was originally designed for Doppler radars in European Alps. The modified algorithm by this study is capable of reading level-II WSR-88D data and dealiasing the radial velocities.

To dealias radial velocity data, the following steps are performed: First, a wind profile is created based on model background, rawindsonde, or wind profiler data. The background radial velocity in radar observation space is calculated from the wind profile, assuming the wind is horizontally homogeneous. Second, the WSR-88D radial velocity is compared with the background radial velocity for a gross check. In this step, aliased radial velocity that needs to be corrected is identified. Third, at each elevation angle, spatial dealiasing is performed. The aliased velocity V_a will be recovered by factored Nyquist velocity V_n,

$$V_d = V_a + 2NV_n \quad , \tag{5}$$

where N is a positive or negative integer whose sign and value are determined by a gate-to-gate shear threshold of $0.4V_n$ (James and Houze 2001). After dealiasing is finished, the radial velocity interpolated to the Cartesian coordinates is thinned to 10 km spacing horizontally and 500 meter vertically.

Figure 3 shows the processed radial velocity at 0.5^{o} elevation angle for KHGX (Fig. 3a) and KLCH (Fig. 3b) at 0000 UTC 13 September 2008. These two radars complement each other by providing scans that are approximately the right angle at the location of Ike's eye. KHGX covers almost all of Ike's eye and eye wall. The outbound radial velocity on the left side of the eye and inbound radial velocity on the right side of the eye reflect the circulation of the hurricane. KLCH covers only about half of eye and eye wall. The outbound radial velocity on the front side of the eye and inbound radial velocity on the back side of the eye also reflect the circulation of the hurricane.

The observation error standard deviation for the radial velocity is set to 2 m s^{-1} during the DA. This error value is similar to the values used in (Dowell; Wicker 2009), (Xu; Gong 2003), and (Xiao et al. 2009Xiao et al. 2009).

c. The data assimilation setup

This paper presents five experiments denoted as NoDA, 3DVARa, 3DVARb, HybridF, and HybridH (Table 1). Experiments differ based on what, if any, assimilation system is used for radar data. The experiments are designed to examine the difference of using flow-dependent versus static background covariance when assimilating the radar data and the impact of DA on the subsequent forecast.

The NoDA experiment did not assimilate any radar data, instead the WRF model initial condition at 0300 UTC 13 September 2008 simply comes from the 1°x1° degree NCEP (National Centers for Environmental Prediction) operational GFS (Global Forecast System) analysis. The 6-hourly GFS analyses also provide the lateral boundary conditions (LBCs).

The "3DVARb" experiment assimilated the radar data using the traditional 3DVAR method where the static background covariance is adopted. The static covariance is generated and further tuned as followed. The NMC method (Parrish; Derber 1992) was first employed to generate the static background covariance statistics based on 12-h and 24-h WRF model forecasts, starting at 00 UTC and 12 UTC every day, during the period from 01 to 15 September 2008. The experiment using the static covariance generated by the above procedure without further tuning is denoted as 3DVARa. Because the default correlation length scales derived from the NMC method reflects mostly large-scale error structures, their direct use may not be appropriate for storm-scale radar DA (Liu et al. 2005). The horizontal correlation length scale of the static covariance is reduced by a factor of 0.3 in experiment 3DVARb and this factor is found to be optimal through experimentations. The 3DVAR experiments contains three stages (Fig. 4a): (1) a single 6-h spinup forecast initialized from the GFS analysis at 1800 UTC, September 12, to produce an initial first guess at 0000 UTC, September 13 for radar DA cycles; (2) assimilation of radial velocity data from KHGX and KLCH radars every 30 minutes for 3 hours; (3) a 21-h deterministic forecast initialized by the analysis at the end of the assimilation cycles in (2). The WRF model boundary conditions for all three stages are also provided by the operational GFS analyses at 6 hourly intervals. Experiment 3DVARb serves as a base line for evaluating the performance of the hybrid method.

Experiments HybridF and HybridH are identical except that the different weighting factors β_1 and β_2 are used in Eq. (2). For HybridF, the full weight is assigned on the flow-dependent ensemble covariance (using β_1 = 0.001 and β_2 = 1.001). For HybridH, the static covariance and the flow-dependent ensemble covariance are equally weighted (β_1 = 0.5 and β_2 = 0.5), i.e., only half of the flow-dependent covariance is used, hence the 'H' in the name. The horizontal correlation scale of static covariance in HybridH is also reduced by a factor of 0.3 as in 3DVARb. Meanwhile, HybridH uses the same flow dependent covariance localization as HybridF, which will be discussed in detail in section 4.a.

Each of the hybrid experiments, HybridF and HybridH, has 40 ensemble members. Similar to the 3DVAR experiments, the hybrid experiments have three stages (Fig. 4b): (1) 6-h ensemble forecasts to spin up a first guess ensemble and provide flow-dependent covariance at the beginning of the radar DA cycles. The initial and boundary conditions for each member are the GFS analysis plus correlated random perturbations following Torn et al. (2006) and Wang et al. (2008a,b); (2) assimilation of perturbed radial velocity data from KHGX and KLCH radars every 30 minutes for 3 hours by variationally minimizing the hybrid cost function, according to the description given in the previous section (see also Fig. 2); (3) a 21-h deterministic forecast initialized from the ensemble mean analysis at the end of the DA cycles in (2). To generate the random perturbations in (1), the random-cv facility in the WRF 3DVAR system is employed (Barker et al. 2004). First, a random control variable vector is created with a normal distribution having a zero mean and unit standard deviation. Then the perturbation control variable vector is transformed to the model space to obtain perturbations to the model state variables including the horizontal wind components, pressure, potential temperature, and mixing ratio of water vapor. The perturbation standard deviations are roughly 1.9 m s^{-1} for the horizontal wind components, 0.6 K for temperature, 0.3 hPa for model pressure perturbation, and 0.9 g kg^{-1} for water vapor mixing ratio and these values are based on the NMC-method-derived background error statistics.

The relaxation method of Zhang et al. (2004) is used for ensemble covariance inflation. The inflated ensemble perturbation $\mathbf{x'}_{new}$ is a weighted average of prior perturbation $\mathbf{x'}_f$ and posterior perturbation $\mathbf{x'}_a$, $\mathbf{x'}_{new} = (1 - b)\, \mathbf{x'}_f + b\, \mathbf{x'}_a$, the relaxation coefficient, denoted as *b,* is set to 0.5.

4. Results and discussion

The analysis increment of the first DA cycle, the cycling process, the final analysis fields, and the deterministic forecasting results will be presented and discussed in this section. The subsection organization roughly follows the experiment flow charts in Fig. 4.

a. Single observation test for vertical localization

Before complete DA experiments are performed, the vertical covariance localization in the hybrid scheme is tested by assimilating a single radial velocity observation. Figure 5 shows the wind speed increment produced by HybridF analyzing a single radial velocity observation located 3176 m above sea level at 0000 UTC 13 September 2008. The innovation (i.e., the observed radial velocity minus forecast ensemble mean valid at 0000 UTC 13 September) for this observation is -38.63 m s^{-1}. Without the vertical localization, nonzero increment reaches the top of the model with relatively noisy increments at the upper levels (Fig. 5a). The horizontal and vertical localization radii of 60 and 3 km, respectively, are used in hybrid experiment HybridF (and in HybridH), and were arrived at after a range of localization scales was tested. Figure 5b shows that with such localizations, the analysis increment is limited to the region within a radius from the observation location, mitigating negative effects of unreliable distant covariance that are unavoidable with a limited-sized ensemble. This single observation test verifies the correctness of our implementation of the vertical localization.

b. Wind increments

To see the differences in analyzing the radar data using flow-dependent and static covariances, the analysis increments from the 3DVAR and hybrid experiments after the first analysis time are compared. We first look at the wind increments and will look at indirectly related cross-variable increments in the next subsection.

Figure 6 shows the wind analysis increments at 850 hPa, at 0000 UTC 13 September 2008, the time of first analysis for 3DVARa, 3DVARb, HybridF, and HybridH. The increment in 3DVARa using the default NMC-method-derived static covariance shows cyclonic and anti-cyclonic increment patterns of rather large scales (Fig. 6a); the cyclonic increment circulation is centered almost 2 degrees off the observation hurricane center to the southsoutheast, while at the hurricane center location the wind increment is mostly easterly. To the north the increment circulation shows an anti-cyclonic pattern. Such cyclonic and anti-cyclonic increments are also found in a previous studies assimilating radar radial velocity data using WRF 3DVAR (e.g., Xiao et al. 2007), but are clearly unrealistic, and do not reflect the fact that a strong vortex exists where the background strongly underestimate the strength of the vortex. The default background error covariance derived from the NMC method is unaware of the hurricane vortex and its spatial correlation scales mostly reflect synoptic scale error structures. The net result is the inappropriately large amount of smoothing of the radar data in the data dense region and inappropriately large spreading of the information outside the data coverage region. The radar data, being collected at high spatial resolution, should be analyzed using much smaller spatial correlation scales. This had been pointed out in Liu et al. (2005) and the use of smaller correlation scales for radar data is a common practice in the ARPS 3DVAR system (e.g., Schenkman et al. 2011).

In 3DVARb, the default horizontal spatial correlation scale is reduced by a factor of 0.3. The resulting wind increment now shows a more or less symmetric cyclonic pattern around the observed center of Ike (Fig. 6b). Compared with 3DVARa, the large increments are more limited to the region of vortex in 3DVARb, and the increment is consistent with the inbound and outbound radial velocity couplets associated with the hurricane vortex as observed by KHGX and KLCH radars (Fig. 3). Such results are more realistic.

In HybridF with full weight given to the flow-dependent covariance, the wind increment also shows a cyclonic pattern centered around the eye of Ike (Fig. 6c), but the increment circulation is less axisymmetric, reflecting the contribution of spatially inhomogeneous flow-dependent covariance. When equal weights are placed on the ensemble covariance and static covariance in HybridH, the wind increments show a pattern that is close to that of 3DVARb, but the increment magnitude is between those of the HybridF and 3DVARb (Fig. 6d).

c. Temperature increments

Because radar radial velocity is the only data type assimilated in this study, any increment in temperature is the result of balance relationship applied (if any) and/or due to cross-covariance in the background error. Figure 7 shows the 850 hPa temperature increments for 3DVARb, HybridF, and HybridH after assimilating radial velocity data for the first cycle. For 3DVARb, negative temperature increments are found in the vortex region, and the magnitude is largest near the hurricane enter (Fig. 7a). Physically, enhanced hurricane vortex circulation should be accompanied by warming of the vortex core region, to give a warmer core vortex; hence the 3DVAR temperature increment is inconsistent with expected hurricane structures. The negative increment is expected of the 3DVAR, because the increment is obtained through a balance relationship between temperature and wind and this relationship reflects the thermal wind relation. More specifically, the 'balanced temperature' increment T_b at a vertical level k, in WRF 3DVAR is related to the stream function ψ by a regression relation, $T_b(k) = \Sigma_l \, G(l,k) \, \psi(l)$, where G is the regression coefficient and the summation is over the vertical index l. Such a regression relation derived using the NMC-method generally reflects hydrostatic, geostrophic, and thermal wind relations (Barker et al. 2004). A colder core at 850 hPa is consistent with an enhanced cyclonic circulation at the 700 hPa seen in Fig. 6. Note that at this distance, the lowest radar beams do not reach below 850 hPa, hence the enhancement of wind is larger above 850 hPa. Therefore the cyclonic wind increment increases with height in the lower atmosphere. We note that negative temperature increment is also seen in the low-level eye region of analyzed hurricanes in previous studies using Airborne Doppler radar data and WRF 3DVAR (e.g., Xiao et al. 2009)

Different from 3DVAR, the temperature increment obtained in HybridF shows positive increments in the eye region (Fig. 7b) and spiral patterns in the eye wall and outer rainband regions. Such much more realistic structures are the result of temperature-wind cross covariances derived from the ensemble, which have knowledge of the vortex as a tropical cyclone. In addition, the magnitude of the temperature increments in HybridF is an order of magnitude larger than that of 3DVARb; the temperature increment in the 3DAR analysis of Xiao et al. (2009) for Hurricane Jeanne (2004) was also weak, reflecting the relative weak thermal wind relationship in 3DVAR.

As the wind increment, the temperature increment from HybridH is in-between those of HybridF and 3DVARb (Fig. 7c). The magnitude is about half that of HybridF. The structure of the increment resembles that of HybridF more but the eye region has negative instead of positive increments. From this aspect, HybridH is poorer than HybridF.

d. Innovation statistics for Vr and minimum sea level pressure in DA cycles

The behaviors of 3DVARb, HybridH, and HybridF are further compared by examining the fit of their analyses and forecasts to Vr observations during the DA cycles. The fit is defined as the root mean square difference (RMSD) between the model state and observations, after the model state is converted to the observed quantities; and such difference is also called observation innovation. Figure 8 shows the RMSDs for Vr and minimum sea level pressure (MSLP) from HybridH, HybridF and 3DVARb. Vr data of both KHGX and KLCH are used in the innovation calculation and for the hybrid, the ensemble mean is used. In all three experiments, the RMSD for Vr is reduced significantly by the analysis within each cycle and the largest reduction occurs in the first analysis cycle at 0000 UTC when the observation innovations are the greatest. In later cycles, the innovations for the analyses remain roughly between 2.5 and 3.5 m s^{-1}, which is reasonable given the 2 m s^{-1} expected observation error. The 30-minute forecasts following each analysis generally increase the Vr innovation by about 2 m s^{-1}, reaching 4-5 m s^{-1} levels. In general, HybridH produces analyses that fit Vr observations tightest while HybridF the least and 3DVARb is in-between. Similar is true of the 30-minute forecasts. It is interesting that the innovations for HybridH are not generally in-between HybridF and 3DVARb, as we saw earlier for the wind and temperature increment fields. We note that such results are possible and can occur, for example, when the observed value is closer to the value of HybridH, that may be in-between the values of HybridF and 3DVAR. The observation innovation statistics can help us to see if the DA system is doing about the right things, but being 'verification' against the same set of observations that is also used in the DA, it cannot really tell us the true quality of the analyses. True measures of the analysis quality require verifications against independent observations or verification of subsequent forecasts, which will be presented later.

Figure 8b shows the fit of the analysis and forecast MSLPs to the best track data from the National Hurricane Center. The best track MSLP is more or less constant during this 3 hour period, being at about 952 hPa. At the beginning of DA cycling (0000 UTC 13 September), the MSLP is about 23 hPa higher than the best track estimate. The reduction of MSLP by HybridF is slightly larger than those of HybridH and 3DVARb in the first analysis. Later on, the reduction by 3DVARb is minimal. Significant reduction in MSLP occurred at 0200 UTC for HybridF, and at 0100 and 0130 UTC for HybridH while in all other cycles the reduction by analysis is minimal. Most of the reduction in MSLP in all cases are actually achieved through adjustment during the forecasting process, with more than 15 hPa reduction achieved during the first analysis cycle between 0000 and 0030 UTC. This is not surprising because wind is the only parameter directly measured, and pressure analysis increments are only achieved through balance relationships and/or cross covariance, which are apparently weak.

We note in general, the MSLP decreases faster in the forecast stages in the hybrid experiments than in 3DVARb. This is consistent with the fact that the hybrid method tends to build a warmer vortex core, and warmer temperature tends to induce a lower surface pressure due to hydrostatic balance. A stronger vortex circulation will also induce lower central pressure due to cyclostrophic balance. During the final 3 cycles, there is clearly over-deepening of the central pressure in HybridH in the forecast stages, resulting in a fall of MSLP that is about 5.5 hPa too low compared to best track. The final analysis MSLP in HybridF is about 2.0 hPa too low, which should be within the uncertainty range of MSLP best track data.

Overall, errors in the maximum surface wind (MSW) and MSLP are greatly reduced after assimilating radar data in all DA experiments. At 0300 UTC 13 September, the end of the DA cycles, the best track MSW and MSLP are 47.5 m s^{-1} and 951 hPa respectively. For 3DVARb, HybridF, and HybridH, after assimilating radar radial wind, the MSW errors are 1, 0.8, and 2.7 m s^{-1} and the MSLP errors are 0.2, 1.9, and 5.6 hPa, respectively. In contrast, for NoDA experiment without assimilating radar data, the MSW error is 9 m s^{-1} and MSLP error is 29 hPa.

e. The analyzed hurricane structures

We examine next the structure of the hurricane at the end of the DA cycles by plotting fields at the surface and in vertical cross sections through the analyzed hurricane center. Figure 9 shows the analyzed mean sea level pressure and surface wind vectors for NoDA, 3DVARb, HybridF and HybridH. Compared with NoDA (Fig. 9a), the analyzed vortex circulations are stronger and the minimum sea level pressure is much lower in 3DVARb, HybridF, and HybridH

(Fig. 9b-d). The low level flow also shows convergence towards the eye wall; such primary hurricane circulations (Willoughby 1990) are captured well by the assimilation of radar radial velocity data.

Figure 10 shows the vertical cross sections of horizontal wind speed and potential temperature for all four experiments. The locations of cross sections are through the analyzed hurricane center and the maximum wind speed as indicated by the thick lines in Fig. 9. The hurricane eye is much wider and the intensity is much weaker in NoDA than in the three radar DA experiments. Given the inner eye pressure deficit, the warm core should extend through the depth of the troposphere based on the hydrostatic approximation (Haurwitz 1935). Compared with the hybrid experiments, 3DVARb shows an unrealistic weak cold core structure at the lower levels. With the downward extruding potential temperature contours in HybridF and HybridH throughout the depth of the plotted domain (Fig. 10c, d), the warm core structure is clear.

The warm core structure is seen even more clearly in the vertical cross sections of horizontal temperature anomaly, which is the deviation from the mean at the pressure levels (Fig. 11). The temperature anomaly in NoDA is very small (less than 2 K, Fig. 11a) while that in 3DVARb, HybridF and HybridH exceeds 8 K, with the maximum anomaly found between 300 and 500 hPa levels (Fig. 11b-d). Such temperature anomalies are expected in hurricanes at similar intensities. Zhu et al. (2004) obtained a maximum anomaly of about 8 K in an 84-h forecast of Hurricane Bonnie (1988) with a MSLP of about 955 hPa. In observational studies, the strength of hurricane warm core has been shown to negatively correlate with MSLP (Halverson et al. 2006; Hawkins; Imbembo 1976).

The near-zero or negative temperature anomaly below 700 hPa is clear in Fig. 11b for 3DVARb. This is related to the negative 3DVARb temperature increment discussed earlier. In

HybridF and HybridH, the positive anomaly extends to the surface (Fig. 11c and 11d). In the latter two, the maximum anomaly is found to be at the inner edge of hurricane eye wall at about 400 hPa, which should be associated with the eye wall warming (LaSeur and Hawkins 1963; Holland 1997).

f. The track and intensity forecasts

To further evaluate the quality of analyses produced by different DA methods, deterministic forecasts initialized from the (ensemble mean in the hybrid cases) analyses at 0300 UTC 13 September, the end of the DA cycles, are launched. The track forecasts are compared in Figure 12a. The center of hurricane is defined as the location of MSLP. The initial track errors at 0300 UTC are less than 20 km for all four experiments. By 0000 UTC 14 September, the track errors are 98, 117, 84, 64 km for NoDA, 3DVARb, HybridF and HybridH respectively. The mean track errors based on the hurricane positions at 6-h interval during the period from 0300 UTC 13 to 0000 UTC 14 September are 41, 57, 41, and 34 km for NoDA, 3DVARb, HybridF, and HybridH respectively. Given that our DA experiments do not include environmental observations, the main effect on the track should come from the changes to the structure and intensity of the analyzed hurricane.

Figure 12b shows the intensity forecasts in terms of MSLP, together with the best track MSLP. At 0300 UTC 13 September, the MSLP errors are 28, 0.2, 2.0, and 5.5 hPa for NoDA, 3DVARb, HybridF and HybridH respectively. NoDA has the largest MSLP error throughout the forecast. The MSLP error in 3DVARb is smaller at the initial time, but becomes larger than those of HybridF and HybridH at the later forecast times. Overall, the forecast MSLP in the two hybrid experiments is closer to the best track MSLP than that of 3DVARb. None of the forecasts capture the slight deepening during the first 3 hours of forecast.

g. Verification of forecasts against Vr observations

The wind forecasts are further verified against observed radar radial velocity data. Figure 13 shows the root mean squared errors (RMSEs, strictly it is RMSD because observations also contain error) of forecast against observed Vr for 3DVARb, HybridF and HybridH. Compared to the best track estimation of wind speed, the radar Vr observations are more reliable. At the initial time of 0300 UTC, the RMSE of 3.5 m s^{-1} from HybridF is slightly larger than those from HybridH (2.6 m s^{-1}) and 3DVARb (2.8 m s^{-1}). After the first hour, the HybridF wind forecast fits the observed radial wind best, especially after 6 hours of forecast where the error in 3DVARb grows much faster and reaching 14.8 m s^{-1} compared to the 8-9 m s^{-1} in the hybrid cases. The much faster error growth in 3DVARb, even though at the initial time its fit to Vr observations is comparable to that of HybridH and better than HybridF, suggests that other model fields in the 3DVARb analysis are dynamically less consistent with the wind field than in the hybrid cases. The slight better forecast in HybridF than in HybridH at 6 hours suggests the fully flow-dependent covariance during the assimilation cycles is beneficial.

h. Evaluation of rainfall forecasts

Rainfall forecasts are evaluated by calculating equitable threat scores (ETSs) of 3-h accumulated precipitation against NCEP Stage IV precipitation analyses (Fig. 14). For the thresholds of 5, 10, and 25 mm/3 hr and all forecast lead times, the hybrid experiments have higher ETSs than 3DVARb. Furthermore, the improvement of the hybrid over 3DVARb increases with precipitation threshold, indicating again the superior quality of the hybrid DA method. In addition, HybridF has slightly higher ETS scores than HybridH for most times and thresholds. The ETS of the hybrid experiments is higher than the NoDA for larger threshold and longer forecast lead times. By further looking at the precipitation patterns, it is found that the precipitation forecasts of HybridF more closely match the observed convective spiral band patterns in the inner core region while 3DVARb produces too much precipitation in the southeast quadrant in the outer band region (the region is within the reflectivity coverage of coastal radars, from which the Stage IV precipitation is estimated, c.f. Fig. 1) and the radius of the inner core eye wall appears larger than observed (Fig. 15). In comparison, the precipitation pattern from NoDA case is poorer than the DA experiments especially for inner rain bands.

5. Summary and conclusions

In this study, the WRF hybrid ensemble-3DVAR data assimilation (DA) system (Wang et al. 2008a,b) is applied for the first time to the assimilation of radial velocity data for a landfalling hurricane. More specifically, radial velocity data from two operational WSR-88D radars along the Gulf of Mexico coast are assimilated over a three-hour period for Hurricane Ike (2008) after it moved into the ranges of the two radar, using an enhanced version of the WRF hybrid DA system. Different from Wang et al. (2008a,b) that employed an ensemble transformation Kalman filter to generate the analysis ensemble, we employ in this study the 'perturbed observation' method used in Hamill and Snyder (2000), which corresponds to the stochastic approach used in the classic stochastic ensemble Kalman filters (Burgers et al. 1998; Houtekamer and Mitchell 1998; Evensen, 2003). Further, we applied vertical localization based on empirical orthogonal functions while continuing to use recursive filters for horizontal localization for the flow-dependent ensemble-estimated background error covariance. The flow-dependent ensemble covariance is incorporated into the 3D variational framework by using the extended control variable method.

The radial velocity data are assimilated every 30 minutes over a 3 hour period. Results mainly from five experiments are presented. A forecast experiment without assimilating any radar data is first carried out to serve as a baseline against which the radar-assimilating experiments are compared; this forecast experiment (NoDA) started directly from the operational GFS analysis at 0300 UTC 13 September 2008, which contained too weak a hurricane vortex. The four radar DA experiments used the WRF 3DVAR using the static covariance derived from the NMC method (3DVARa), the WRF 3DVAR using further tuned static covariance (3DVARb), the hybrid DA system with purely flow-dependent background covariance (HybridF), as well as half static and half flow-dependent covariance (HybridH), respectively. In the tuned 3DVAR experiment (3DVARb) as well as HybridH, the horizontal spatial correlation scale in the static covariance derived from the NMC-method is reduced by a factor of 0.3 to produce much more realistic wind increments than the default scale (in 3DVARa). The results of analyses and forecasts from the five experiments are inter-compared and verified against best track data, radar wind measurements and precipitation data. The main conclusions are summarized in the following.

(1) When using the default background error covariance derived from the NMC method (experiment 3DVARa), WRF 3DVAR produces unrealistic wind increments from radial velocity (Vr) data of two Doppler radars having good coverage of the hurricane vortex. With a reduced spatial covariance correlation scale (in 3DVARb), the wind increments properly reflect the hurricane primary circulation.

(2) The largest wind increments are obtained in the first few analysis cycles. The increments of the hybrid scheme with full flow-dependent covariance (in HybridF) produce a less axisymmetric increment circulation than 3DVARb and HybridH.

(3) HybridF produces the most realistic temperature increments with positive values at the hurricane center, corresponding to the warm core structure, while 3DVARb produces much

weaker and smoother temperature increments that are negative at the center of hurricane. At the end of assimilation cycles, negative temperature anomalies are found below 700 hPa in the eye region of 3DVARb analysis while the hybrid analyses show deep warm core structures.

(4) All three DA experiments are able to create analyses that fit the Vr data well, and the error reduction by analysis is the largest in the first analysis cycle. The analysis fit to Vr observations is the closest in HybridH and the least close in HybridF in general during the DA cycles. Most of the minimum sea level pressure (MSLP) reduction is achieved through model adjustment during the forecast step of the assimilation cycles, and the MSLP is within 2.5 hPa of the best track value after 4 analysis cycles of 30 minute interval. HybridH over-analyzes the final MSLP by about 5.6 hPa while those of 3DVARb and HybridF are within 0.2 and 1.9 hPa of the best track data, respectively.

(5) The hybrid experiments improve the Ike track forecast slightly, over the track forecast by NoDA starting from the GFS analysis. 3DVARb slightly degrades the track forecast. All radar DA experiments produce MSLP forecasts that are generally within 8 hPa of the best track data, with 3DVARb predicting the weakest hurricane among the DA experiments. The NoDA experiment from GFS analysis starts with an error of nearly 30 hPa in MSLP and ends with an error of a little over 10 hPa when Ike was much weaker after landfall.

(6) The most interesting is that the fit of forecast radial velocity to radar observations during the first 6 hours of forecast is much worse with 3DVARb than with HybridF and HybridH, having RMSEs of about 14.8, 8.5 and 9.3 m s^{-1} for the three, respectively, at the 6-hour forecast, even though the final analysis of 3DVARb fits the observations closer than that of HybridF (about 2.8 and 3.5 m s^{-1}, respectively). The forecast results indicate that the overall quality of hybrid analyses is better than that of 3DVARb, producing more dynamically consistent

state estimations that lead to later slower error growth during forecast. The forecast error of HybridF is slightly lower than that of HybridH starting from hour three. In the absence of independent observations for verification during the data assimilation period, the quality of an analysis is best measured by the accuracy of the ensuring forecast.

(7) The equitable threat scores (ETSs) for 3-hour accumulated precipitation forecasts in the hybrid experiments are higher than those of 3DVARb for the thresholds and lead times considered, and the improvement increases with precipitation threshold, indicating again the superior quality of the hybrid DA method. Among the hybrid experiments, HybridF produced slightly better ETSs than HybridH most times.

(8) The results of this study also show positive impacts of assimilating radar data for hurricane initialization, and the hybrid-method-analyzed hurricane has kinematic and thermodynamic structures that are consistent with tropical cyclone conceptual models.

Finally a point worth noting: the inclusion of static background covariance in HybridH in general did not improve the results over HybridF; i.e., the use of flow-dependent covariance in full in general gives better results. Earlier studies suggested that the optimal combination of the static and flow-dependent covariance depends on their relative quality (Hamill and Snyder 2000; Wang et al. 2007a). Our results suggest that for hurricanes and radar data, there is little benefit of including static covariance because static covariance is not capable of appropriately reflecting the mesoscale and convective-scale nature of hurricanes, and because of the dominant scales of motion that radar data measure.

We also note that this study represents the first attempt of applying a variational-ensemble hybrid data assimilation method to hurricane and radar data assimilation. While the results are positive and encouraging, more robust conclusions will need to be drawn by testing the method on many more cases. Other observational data should also be assimilated together to improve the hurricane environment as well. These are topics for future research.

Acknowledgements: This research was primarily supported by a subcontract to a grant from the Mississippi State University led by Dr. Haldun Karan. The first author also acknowledges Dr. Curtis N. James for radar data processing, Shizhang Wang, Alex Schenkman, and Dr. Robin Tanamachi for helpful discussions and assistance with initial drafts. This work was also supported by NSF grant AGS-0802888 and DOD-ONR grant N00014-10-1-0775, NOAA THOPREX grant NA08OAR4320904, NASA NIP grant NNX10AQ78G. The experiments were conducted on a supercomputer at the Mississippi State University.

References

Barker, D. M., W. Huang, Y. R. Guo, A. J. Bourgeois, and Q. N. Xiao, 2004: A Three-Dimensional Variational Data Assimilation System for MM5: Implementation and Initial Results. *Monthly Weather Review*, 132, 897-914.

Buehner, M., 2005: Ensemble-derived stationary and flow-dependent background-error covariances: Evaluation in a quasi-operational NWP setting. *Quart. J. Roy. Meteor. Soc.*, 131, 1013-1043.

---, P. L. Houtekamer, C. Charette, H. L. Mitchell, and B. He, 2010a: Intercomparison of variational data assimilation and the ensemble Kalman filter for global deterministic NWP. Part I: Description and single-observation experiments. *Mon. Wea. Rev.*, 138, 1550-1566.

---,--,--,--, and --, 2010b: Intercomparison of variational data assimilation and the ensemble Kalman filter for global deterministic NWP. Part II: One-month experiments with real observations. *Mon. Wea. Rev.*, 138, 1567-1586.

Burgers, G., P. J. van Leeuwen, and G. Evensen, 1998: Analysis scheme in the ensemble Kalman filter, *Mon. Wea. Rev*., 126, 1719--1724.

Dong, J., and M. Xue, 2012: Coastal WSR-88D Radar Data Assimilation with Ensemble Kalman Filter for Analysis and Forecast of Hurricane Ike (2008). *Quart. J. Roy. Meteor. Soc.,* Conditionally accepted.

Dowell, D. C. and L. J. Wicker, 2009: Additive Noise for Storm-Scale Ensemble Data Assimilation. *J Atmos Ocean Tech*, 26, 911-927.

Dudhia, J., 1989: Numerical study of convection observed during the Winter Monsoon Experiment using a mesoscale two-dimensional model. J. Atmos. Sci., 46, 3077-3107.

Etherton, B. J., and C. H. Bishop, 2004: The resilience of hybrid ensemble/3D-Var analysis schemes to model error and ensemble covariance error. *Mon. Wea. Rev.,*132, 1065-1080.

Evensen, G., 2003: The ensemble Kalman filter: Theoretical formulation and practical implementation. *Ocean Dynamics*, 53, 343-367.

Grell, G. A. and D. Devenyi, 2002: A generalized approach to parameterizing convection combining ensemble and data assimilation techniques. *Geophys Res Lett*, 29(14), Article 1693.

Halverson, J. B., J. Simpson, G. Heymsfield, H. Pierce, T. Hock, and L. Ritchie, 2006: Warm core structure of Hurricane Erin diagnosed from high altitude dropsondes during CAMEX-4. *J Atmos Sci*, 63, 309-324.

Hamill, T. M. and C. Snyder, 2000: A hybrid ensemble Kalman filter-3D variational analysis scheme. *Mon. Wea. Rev.*, 128, 2905-2919.

Hamill, T. M., J. S. Whitaker, M. Fiorino, and S. G. Benjamin, 2011: Global ensemble predictions of 2009's tropical cyclones initialized with an ensemble Kalman filter. Mon. Wea. Rev., 139, 668-688.

Haurwitz, B., 1935: The height of tropical cyclones and the eye of the storm. *Mon. Wea. Rev.*, 63, 45-49.

Hawkins, H. F. and S. M. Imbembo, 1976: The structure of a small, intense hurricane-Inez 1966. *Mon. Wea. Rev.*, 104, 418-442.

Holland, G. J.,, 1997: The maximum potential intensity of tropical cyclones. *J. Atmos. Sci.*, 54, 2519-2541.

Hong, S.-Y., J. Dudhia, and S.-H. Chen, 2004: A revised approach to ice microphysical processes for the bulk parameterization of clouds and precipitation. *Monthly Weather*

Review, 132, 103-120.

Houtekamer, P. L., and H. L. Mitchell, 1998: Data Assimilation Using an Ensemble Kalman Filter Technique. *Mon. Wea. Rev.*, 126, 796–811.

James, C. N. and R. A. Houze, 2001: A real-time four-dimensional Doppler dealiasing scheme. *J Atmos Ocean Tech*, 18, 1674-1683.

Kleist, D., K. Ide, J. Whitaker, J. C. Derber, D. Parrish and X. Wang, 2011: Expanding the GSI based hybrid ensemble-variational system to include more flexible parameter settings. Paper J16.4. AMS Annual meeting, Seattle, WA. Jan. 23-27, 2011

Kurihara, Y., M. A. Bender, R. E. Tuleya, and R. Ross, 1995: Improvements in the GFDL hurricane prediction system. *Mon. Wea. Rev.,* 123, 2791-2801.

La Seur, N. E., and H. F. Hawkins, 1963: An analysis of Hurricane Cleo (1958) based on data from research reconnaissance aircraft. *Mon. Wea. Rev.*, 91, 694-709.

Li, J., and H. Liu, 2009: Improved hurricane track and intensity forecast using singlefield-of-view advanced IR sounding measurements. *Geophy. Res. Lett.*, 36, L11813.

Liu, Q., T. Marchok, H.-L. Pan, M. Bender, and S. J. Lord, 2000: Improvements in hurricane 2 initialization and forecasting at NCEP with global and regional (GFDL) models. Tech. rep., 3 NOAA Tech. Procedures Bull. 472, 7 pp., Camp Springs, MD.

Liu, S., M. Xue, J. Gao, and D. Parrish, 2005: Analysis and impact of super-obbed Doppler radial velocity in the NCEP grid-point statistical interpolation (GSI) analysis system. *Extended abstract, 17th Conf. Num. Wea. Pred.*, Washington DC, Amer. Meteor. Soc., 13A.4.

Lorenc, A., 2003: The potential of the ensemble Kalman filter for NWP - a comparison with 4D-Var. *Quart. J. Roy. Meteor. Soc.*, 129, 3183-3204.

Mlawer, E. J., S. J. Taubman, P. D. Brown, M. J. Iacono, and S. A. Clough, 1997: Radiative transfer for inhomogeneous atmospheres: RRTM, a validated correlated-k model for the longwave. *J. Geophys. Res.*, 102, 16663-16682.

Noh, Y., W. G. Cheon, S. Y. Hong, and S. Raasch, 2003: Improvement of the K-profile model for the planetary boundary layer based on large eddy simulation data. *Bound-Lay Meteorol*, 107, 401-427.

Parrish, D. F. and J. C. Derber, 1992: The National Meteorological Center's spectral statistical-interpolation analysis system. *Mon. Wea. Rev.*, 120, 1747-1763.

Pielke, R. A., J. Gratz, C. W. Landsea, D. Collins, M. A. Saunders, and R. Musulin, 2008: Normalized hurricane damage in the United States: 1900-2005. *Natural hazards Review*, 29-42.

Schenkman, A., M. Xue, A. Shapiro, K. Brewster, and J. Gao, 2011: The analysis and prediction of the 8-9 May 2007 Oklahoma tornadic mesoscale convective system by assimilating WSR-88D and CASA radar data using 3DVAR. *Mon. Wea. Rev.*, 139, 224-246.

Skamarock, W. C., J. B. Klemp, J. Dudhia, D. O. Gill, D. M. Barker, M. Duda, X.-Y. Huang, W. Wang and J. G. Powers, 2008: A Description of the Advanced Research WRF Version 3. NCAR Technical Note TN-475+STR, 113 pp .

Torn, R. D., and G. J. Hakim, 2009: Initial condition sensitivity of western-Pacific extratropical transitions determined using ensemble-based sensitivity analysis. *Mon. Wea. Rev.* 137, 3388-3406.

−, −, and C. Snyder, 2006: Boundary conditions for limited-area ensemble Kalman filters. Mon. Wea. Rev., 134, 2490–2502.

Wang, X., T. M. Hamill, J. S. Whitaker and C. H. Bishop, 2007a: A comparison of hybrid ensemble transform Kalman filter-OI and ensemble square-root filter analysis schemes. *Mon. Wea. Rev.*, 135, 1055-1076.

---, C. Snyder, and T. M. Hamill, 2007b: On the theoretical equivalence of differently proposed ensemble/3D-Var hybrid analysis schemes. *Mon. Wea. Rev.*, 135, 222-227.

---, D. M. Barker, C. Snyder, and T. M. Hamill, 2008a: A Hybrid ETKF-3DVAR Data Assimilation Scheme for the WRF Model. Part I: Observing system simulation experiment. *Mon. Wea. Rev.*, 136, 5116-5131.

---,--,--,and --, 2008b: A hybrid ETKF-3DVAR data assimilation scheme for the WRF model. Part II: Real observation experiment. *Mon. Wea. Rev.*, 136, 5132-5147.

---, T. M. Hamill, J. S. Whitaker, C. H. Bishop, 2009: A comparison of the hybrid and EnSRF analysis schemes in the presence of model error due to unresolved scales. *Mon. Wea. Rev.*, 137,3219-3232

---, 2010: Incorporating ensemble covariance in the Gridpoint Statistical Interpolation (GSI) variational minimization: a mathematical framework. *Mon. Wea. Rev.*, 138,2990-2995.

---, 2011: Application of the WRF hybrid ETKF-3DVAR data assimilation system for hurricane track forecasts. *Wea. Forecasting*, 26, 868-884.

----, T. Lei, J. Whitaker, D. Parrish, and D. Kleist, 2011: GSI-based hybrid ensemble-variational data assimilation system for the Global Forecast system model: 3DVAR-based hybrid and ensemble 4DVAR. Paper J16.5. AMS Annual meeting, Seattle, WA. Jan. 23-27, 2011.

Whitaker, J., D. Kleist, X. Wang and T. Hamill, 2011: Tests of a hybrid variational-ensemble global assimilation system for hurricane prediction. Paper J16.2. AMS annual meeting, 2011, Seattle, WA.

Willoughby, H. E., 1990: Temporal changes in the primary circulationin tropical cyclones. *J. Atmos. Sci.,* 47, 242–264.

Xiao, Q. N., and J. Sun, 2007: Multiple radar data assimilation and short-range quantitative precipitation forecasting of a squall line observed during IHOP_2002. *Mon.Wea.Rev.*, 135, 3381-3404.

---, X. Y. Zhang, C. Davis, J. Tuttle, G. Holland, and P. J. Fitzpatrick, 2009: Experiments of Hurricane Initialization with Airborne Doppler Radar Data for the Advanced Research Hurricane WRF (AHW) Model. *Mon Weather Rev*, 137, 2758-2777.

Xu, Q. and J. D. Gong, 2003: Background error covariance functions for Doppler radial-wind analysis. *Q J Roy Meteor Soc*, 129, 1703-1720.

Zhang, F., C. Snyder, and J. Sun, 2004: Impacts of initial estimate and observations on the convective-scale data assimilation with an ensemble Kalman filter. *Mon. Wea. Rev.*, 132, 1238-1253.

Zhang, F., Y. Weng, J. A. Sippel, Z. Meng, and C. H. Bishop, 2009: Cloud-resolving hurricane initialization and prediction through assimilation of Doppler radar observations with an ensemble Kalman filter. *Mon. Wea. Rev.*, 137, 2105-2125.

Zhang, F., M. Zhang and J. A. Hansen, 2009: Coupling ensemble Kalman filter with four-dimensional variational data assimilation. *Advances in Atmospheric Sciences ,* 26, 1-8

Zhao, K. and M. Xue, 2009: Assimilation of coastal Doppler radar data with the ARPS 3DVAR and cloud analysis for the prediction of Hurricane Ike (2008). *Geophy. Res. Lett.*, 36, L12803.

Zhu, T., D.-L. Zhang, and F. Weng, 2004: Numerical simulation of Hurricane Bonnie (1998). Part I: Eyewall evolution and intensity changes. *Mon. Wea. Rev.*, 132, 225-241.

Zou, X. L. and Q. N. Xiao, 2000: Studies on the initialization and simulation of a mature hurricane using a variational bogus data assimilation scheme. *J. Atmos. Sci.*, 57, 836-860.

Zupanski, M., 2005: Maximum Likelihood Ensemble Filter: Theoretical Aspects. *Mon. Wea. Rev.*, 133, 1710-1726.

Table Caption

Table 1. List of experiments

Figure Captions

Fig. 1. The WRF model domain and National Hurricane Center best track positions for Hurricane Ike (2008) from 1800 UTC 12 to 0000 UTC 14 September 2008. Also indicated are the Houston, Texas (KHGX) and Lake Charles, Louisiana (KLCH) WSR-88D radar locations (asterisks) and maximum range (300 km for radial velocity and 460 km for the reflectivity) coverage circles.

Fig. 2. Schematic diagram of the hybrid ensemble-3DVAR forecast-analysis cycle for a hypothetical three-member ensemble. Each member assimilates the observations containing a different set of perturbations.

Fig. 3. The radial velocity (interval of 20 m s-1) at 0.5o elevation angle from (a) KHGX and (b) KLCH WSR-88D radars at 0000 UTC 13 September 2008. Black dot is for NHC best-track position of Hurricane Ike (2008) at this time. Asterisks are for radar locations.

Fig. 4. The flow charts for (a) NoDA experiment, (b) 3DVAR experiments (3DVARa and 3DVARb), and (b) hybrid experiments (HybridF and HybridH).

Fig. 5. The vertical cross section of the wind speed increment (interval of 5 m s-1) using a single KHGX radar radial velocity data located at (28.4oN, 93.7oW, 3176 m) with an innovation of -38.63 m s-1 using the configurations of experiment HybridF but (a) without and (b) with vertical localization at 0000 UTC 13 September 2008.

Fig. 6. The 700 hPa wind analysis increments (m s-1) for (a) 3DVARa, (b) 3DVARb, (c) HybridF, and (d) HybridH at 0000 UTC 13 September 2008.

Fig. 7. The 850 hPa temperature analysis increments for (a) 3DVARb (at intervals of 0.3 K), (b) HybridF (at intervals of 0.7 K), and (c) HybridH (at intervals of 0.3 K), at 0000 UTC 13 September 2008.

Fig. 8. The forecast and analysis (sawtooth pattern during DA cycling) of (a) RMSD of radial velocity (m s-1), and (b) the minimum sea level pressures (hPa) together with the NHC best track estimate, for 3DVARb, HybridF, and HybridH from 0000 to 0300 UTC 13 September 2008.

Fig. 9. The analyzed sea level pressure (interval of 5 hPa, solid contours) and the surface wind vectors (m s-1) for (a) NoDA, (b) 3DVARb, (c) HybridF, and (d) HybridH at 0300 UTC 13 September 2008. The thick solid line indicates the vertical cross section location in Fig. 10 and Fig. 11.

Fig. 10. Vertical cross sections of analyzed horizontal wind speed (interval of 10 m s-1, shaded) and potential temperature (interval of 5 K, solid contours) for (a) NoDA, (b) 3DVARb, (c) HybridF, and (d) HybridH, at 0300 UTC 13 September 2008.

Fig. 11. Vertical cross sections of analyzed temperature anomalies (interval of 2 K) for (a) NoDA, (b) 3DVARb, (c) HybridF, and (d) HybridH, at 0300 UTC 13 September 2008.

Fig. 12. Deterministic forecast hurricane (a) tracks and (b) minimum sea level pressure (hPa) by NoDA, 3DVARb, HybridF, and HybridH as compared to NHC best track estimates from 0300 UTC 13 through 0000 UTC 14 September 2008.

Fig. 13. Deterministic forecast RMSEs of Vr (m s-1) by 3DVARb, HybridF, and HybridH from 0300 to 0900 UTC 13 September 2008.

Fig. 14. The equitable threat scores for 3 h accumulated forecast precipitation by NoDA, 3DVARb, HybridF, and HybridH at thresholds (a) 5 mm, (b) 10 mm, and (c) 25 mm, verified against NCEP Stage-IV precipitation analyses valid at 0600, 0900, 1200, and 1500 UTC 13 September 2008.

Fig. 15 Three-hour accumulated precipitation (mm) by (1st column) NCEP Stage-IV precipitation analyses, (2nd column) NoDA, (3rd column) 3DVARb, and (4th column) HybridF valid at (top) 0600 and (bottom) 0900 UTC 13 September 2008.

Table 1. List of experiments

Experiment	Description
NoDA	No radar data assimilation. WRF model initial condition interpolated from NCEP 1^{o}x1^{o} analysis
3DVARa	Radar DA using WRF 3DVAR with static covariance from NMC method
3DVARb	Same as 3DVARa, except the horizontal spatial correlation in the static covariance is multiplied by 0.3.
HybridF	Radar DA using hybrid method with full weight given to flow dependent covariance, with $\beta_1 = 0.001$ and $\beta_2 = 1.001$ in Eq. (1)
HybridH	Hybrid method with equal weight given to static covariance (which is the same as 3DVARb) and flow-dependent covariance, with $\beta_1 = 0.5$ and $\beta_2 = 0.5$ in Eq. (1)

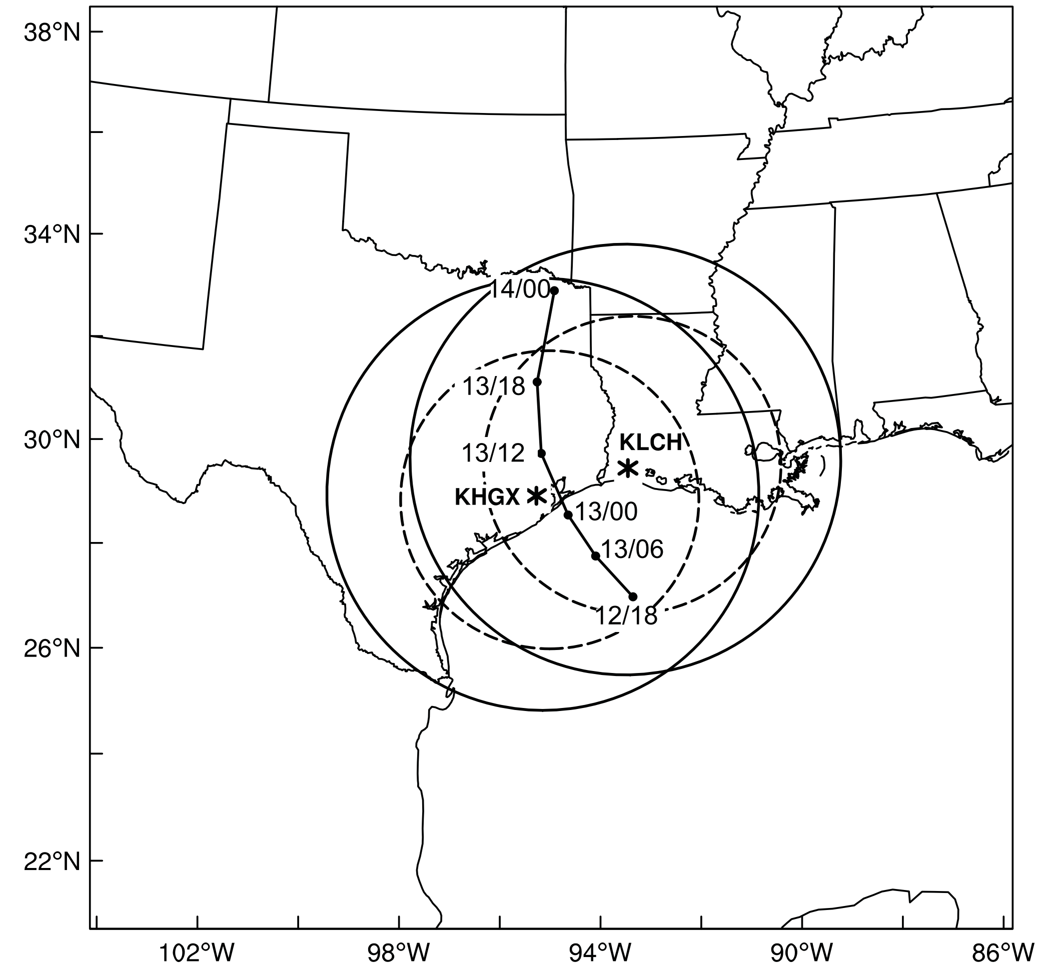

Fig. 1. The WRF model domain and National Hurricane Center best track positions for Hurricane Ike (2008) from 1800 UTC 12 to 0000 UTC 14 September 2008. Also indicated are the Houston, Texas (KHGX) and Lake Charles, Louisiana (KLCH) WSR-88D radar locations (asterisks) and maximum range (300 km for radial velocity and 460 km for the reflectivity) coverage circles.

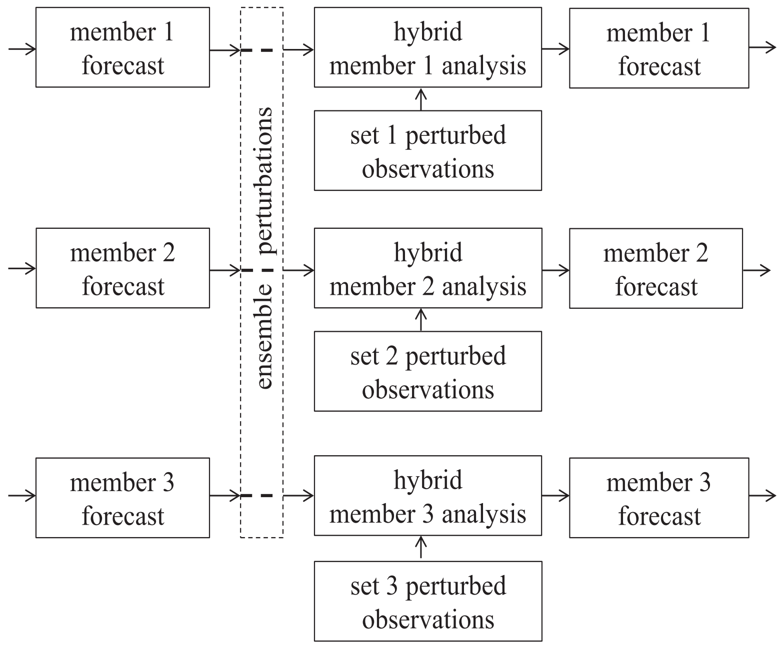

Fig. 2. Schematic diagram of the hybrid ensemble-3DVAR forecast-analysis cycle for a hypothetical three-member ensemble. Each member assimilates the observations containing a different set of perturbations.

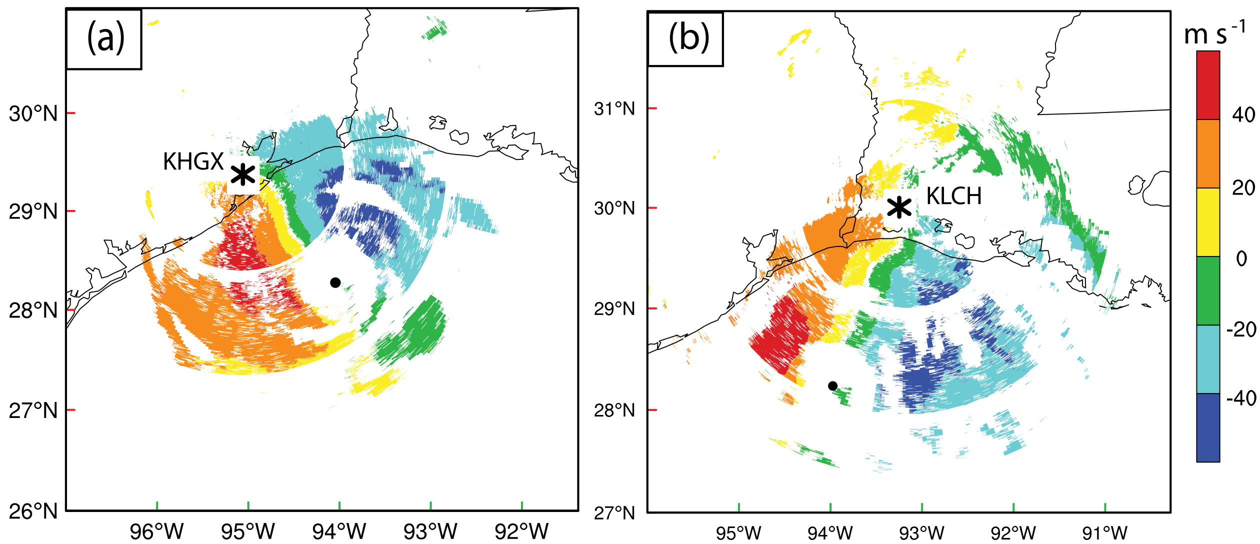

Fig. 3. The radial velocity (interval of 20 m s^{-1}) at 0.5^{o} elevation angle from (a) KHGX and (b) KLCH WSR-88D radars at 0000 UTC 13 September 2008. Black dot is for NHC best-track position of Hurricane Ike (2008) at this time. Asterisks are for radar locations.

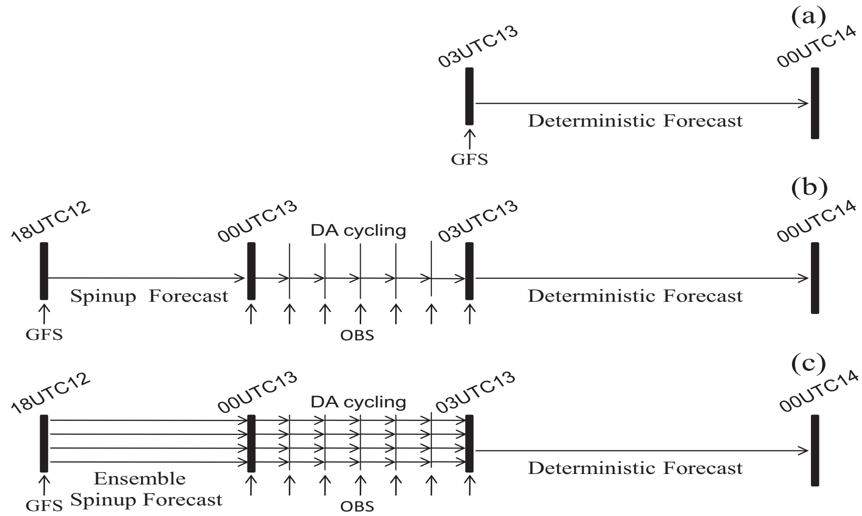

Fig. 4. The flow charts for (a) NoDA experiment, (b) 3DVAR experiments (3DVARa and 3DVARb), and (b) hybrid experiments (HybridF and HybridH).

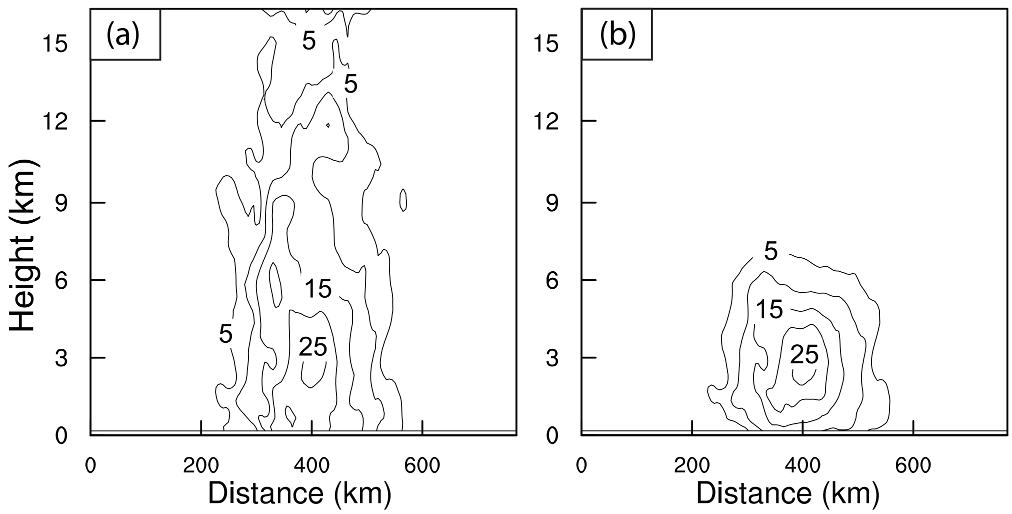

Fig. 5. The vertical cross section of the wind speed increment (interval of 5 m s^{-1}) using a single KHGX radar radial velocity data located at (28.4^{o}N, 93.7^{o}W, 3176 m) with an innovation of -38.63 m s^{-1} using the configurations of experiment HybridF but (a) without and (b) with vertical localization at 0000 UTC 13 September 2008.

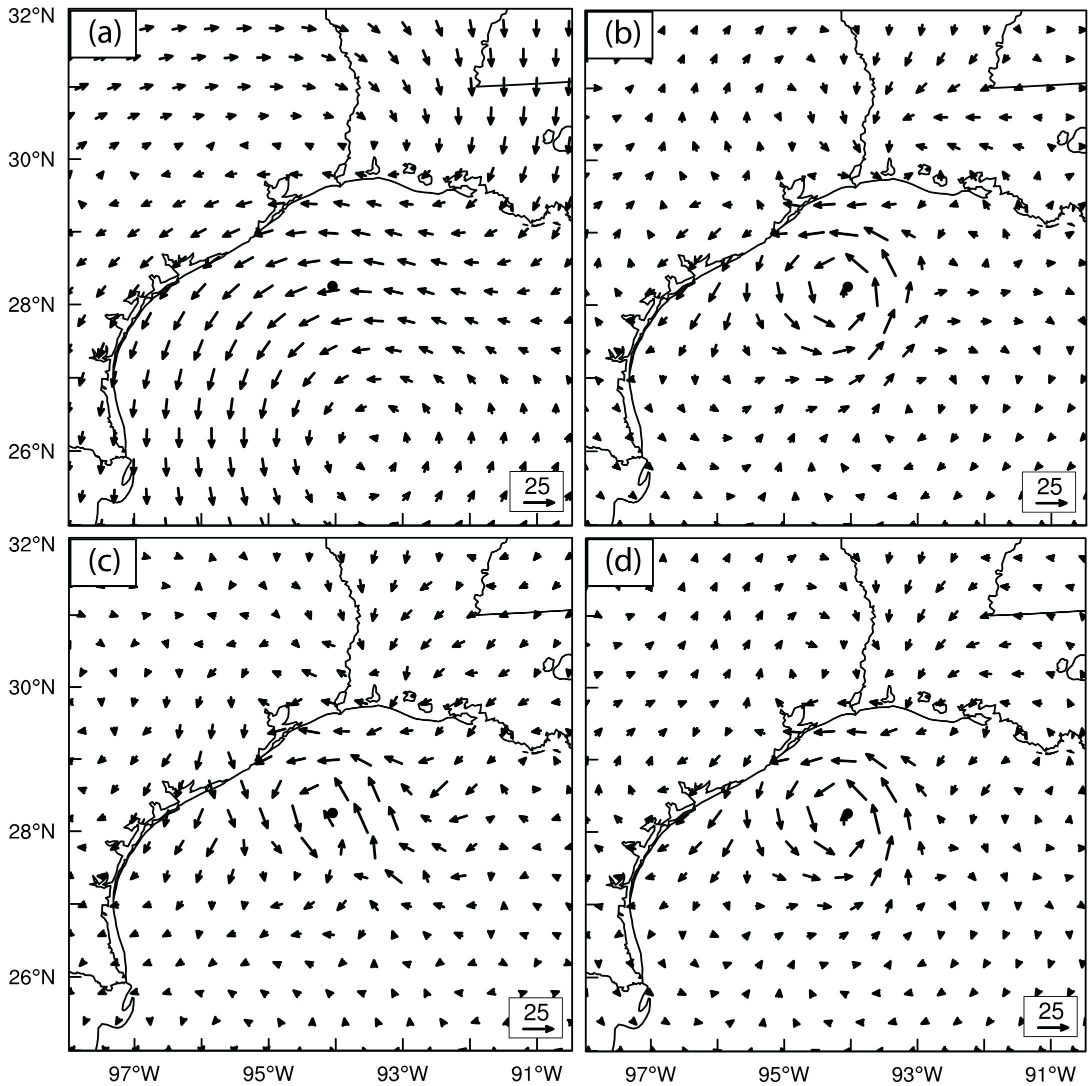

Fig. 6. The 700 hPa wind analysis increments (m s^{-1}) for (a) 3DVARa, (b) 3DVARb, (c) HybridF, and (d) HybridH at 0000 UTC 13 September 2008.

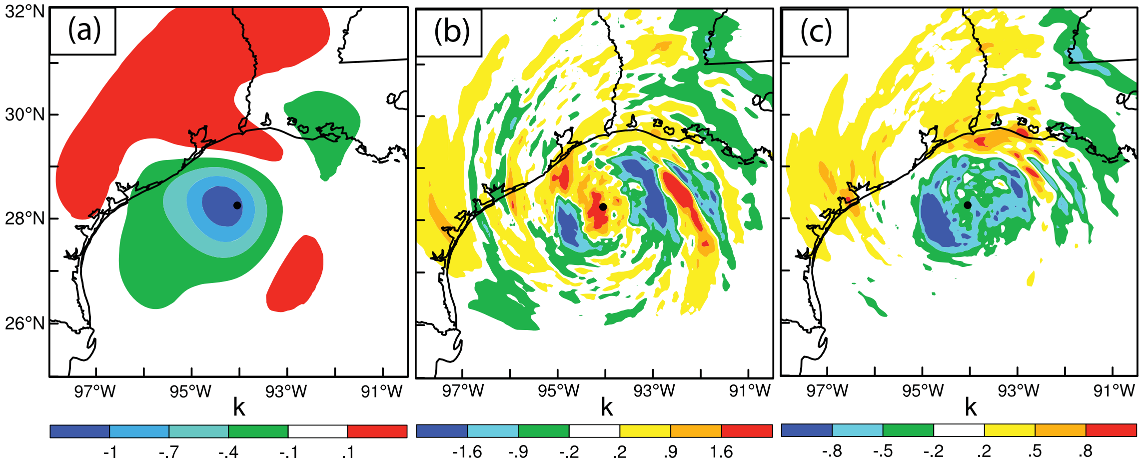

Fig. 7. The 850 hPa temperature analysis increments for (a) 3DVARb (at intervals of 0.3 K), (b) HybridF (at intervals of 0.7 K), and (c) HybridH (at intervals of 0.3 K), at 0000 UTC 13 September 2008.

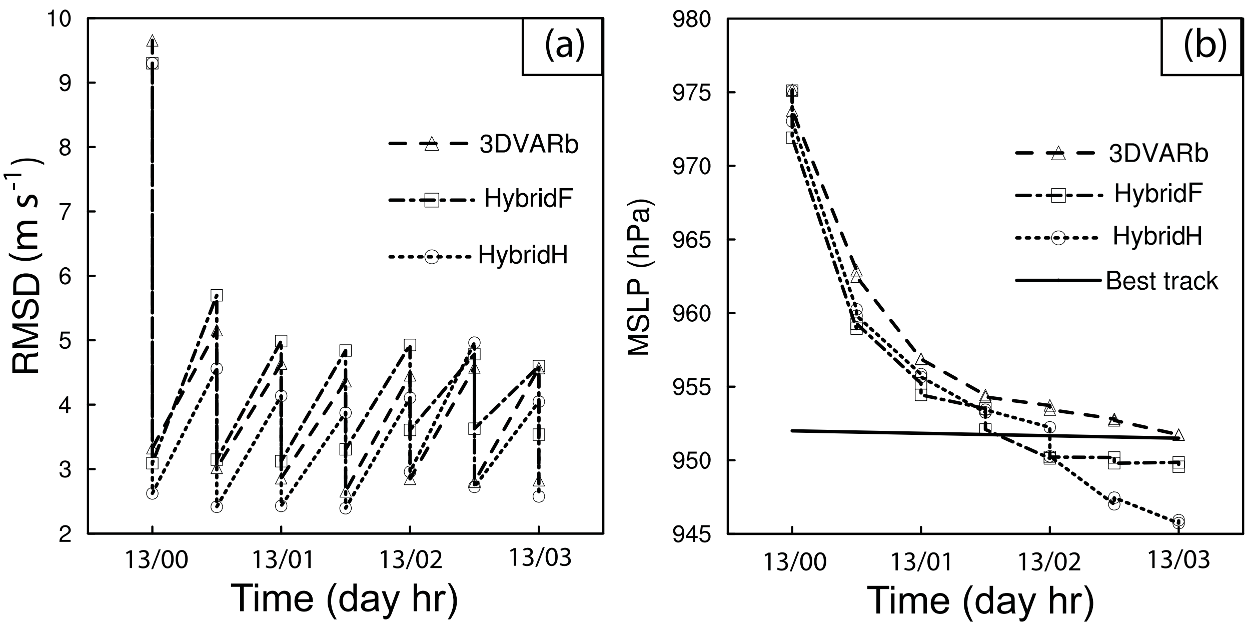

Fig. 8. The forecast and analysis (sawtooth pattern during DA cycling) of (a) RMSD of radial velocity (m s^{-1}), and (b) the minimum sea level pressures (hPa) together with the NHC best track estimate, for 3DVARb, HybridF, and HybridH from 0000 to 0300 UTC 13 September 2008.

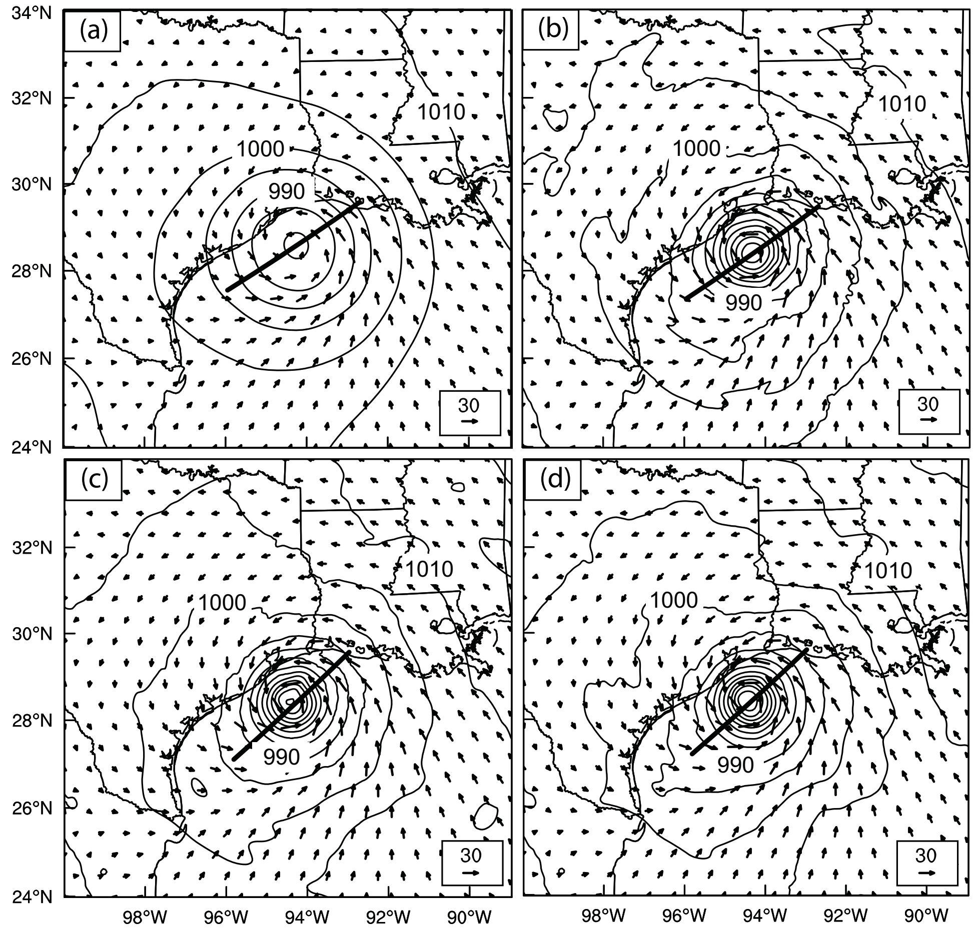

Fig. 9. The analyzed sea level pressure (interval of 5 hPa, solid contours) and the surface wind vectors (m s^{-1}) for (a) NoDA, (b) 3DVARb, (c) HybridF, and (d) HybridH at 0300 UTC 13 September 2008. The thick solid line indicates the vertical cross section location in Fig. 10 and Fig. 11.

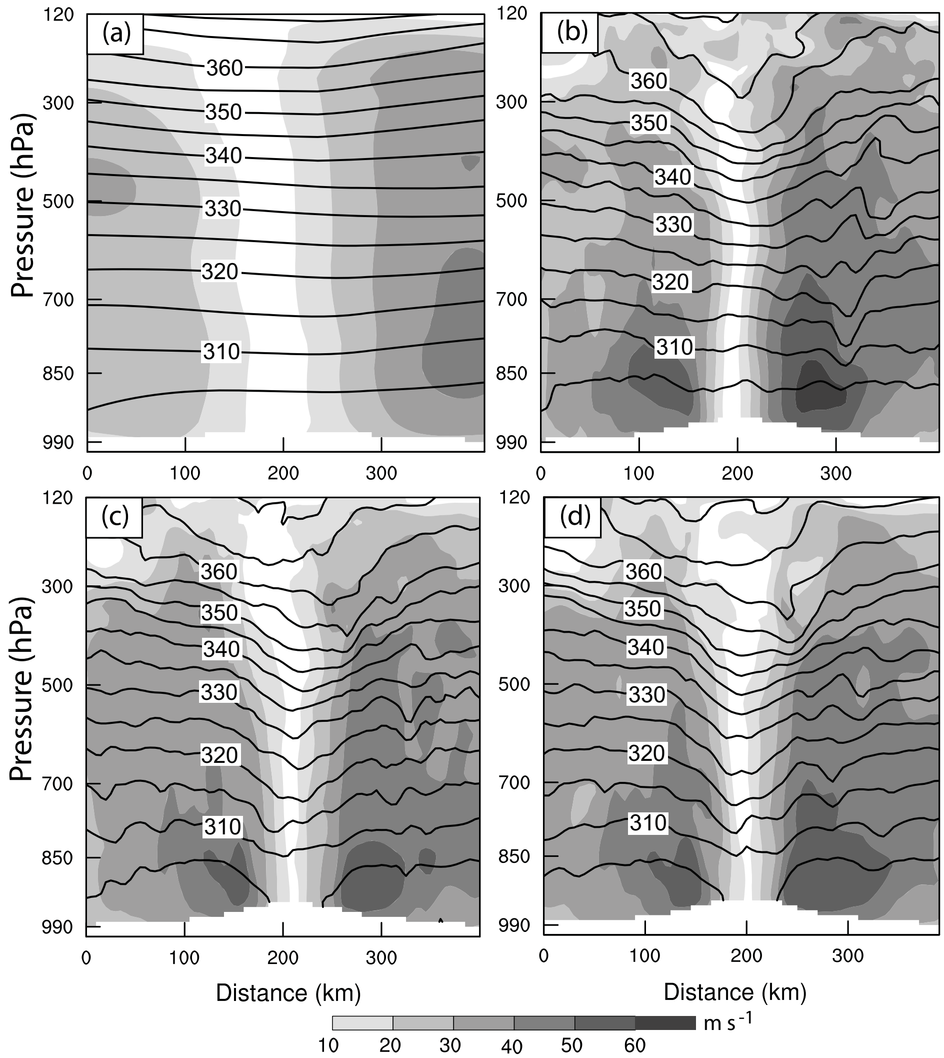

Fig. 10. Vertical cross sections of analyzed horizontal wind speed (interval of 10 m s^{-1}, shaded) and potential temperature (interval of 5 K, solid contours) for (a) NoDA, (b) 3DVARb, (c) HybridF, and (d) HybridH, at 0300 UTC 13 September 2008.

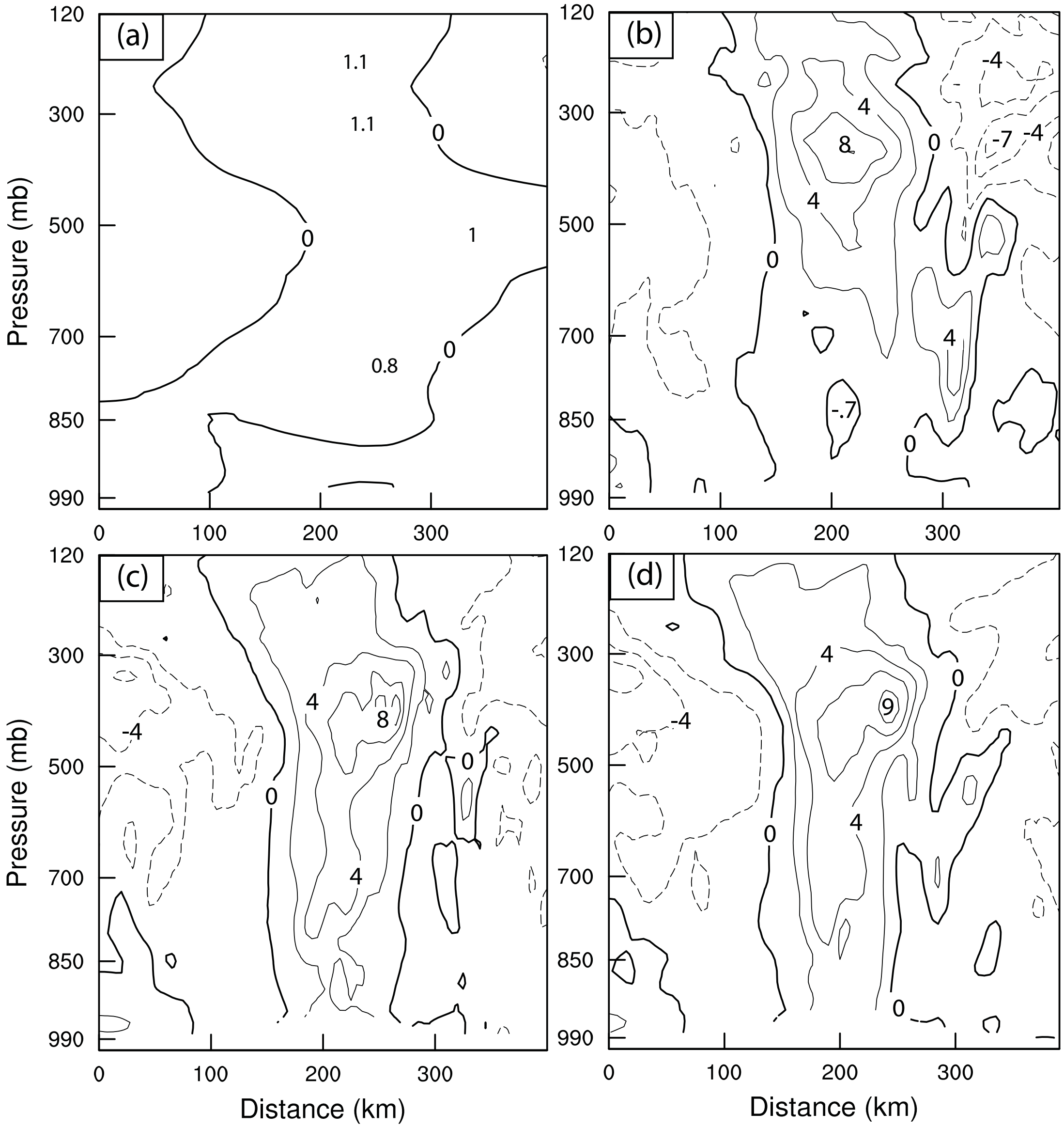

Fig. 11. Vertical cross sections of analyzed temperature anomalies (interval of 2 K) for (a) NoDA, (b) 3DVARb, (c) HybridF, and (d) HybridH, at 0300 UTC 13 September 2008.

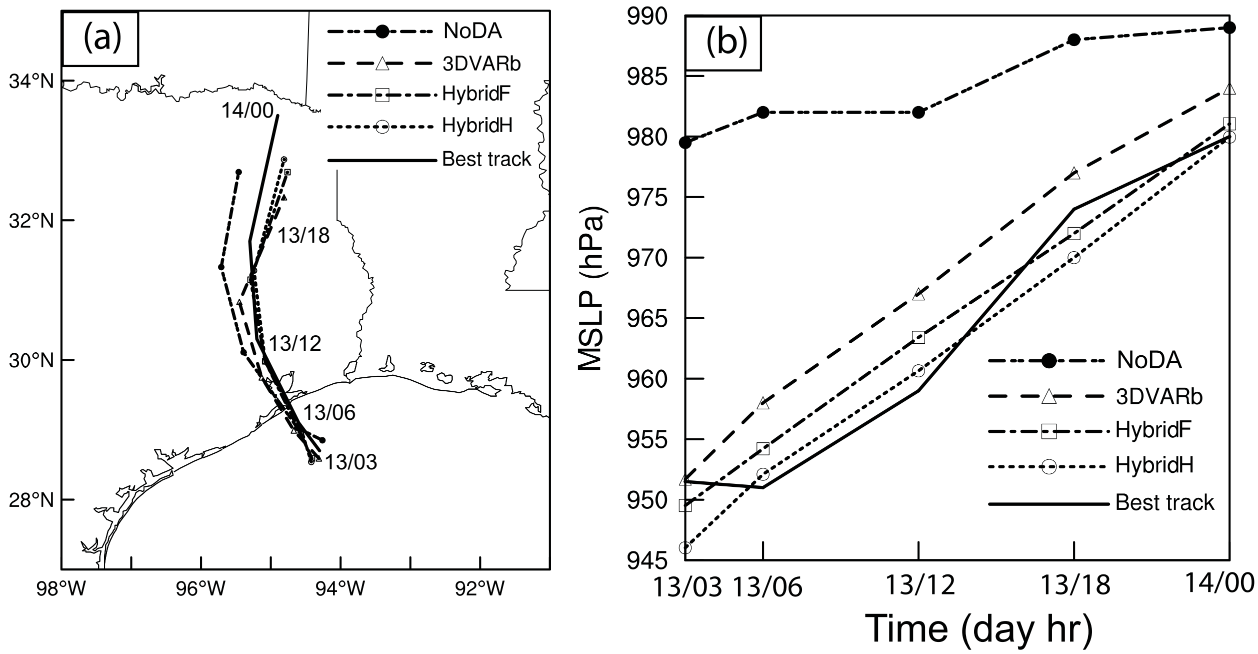

Fig. 12. Deterministic forecast hurricane (a) tracks and (b) minimum sea level pressure (hPa) by NoDA, 3DVARb, HybridF, and HybridH as compared to NHC best track estimates from 0300 UTC 13 through 0000 UTC 14 September 2008.

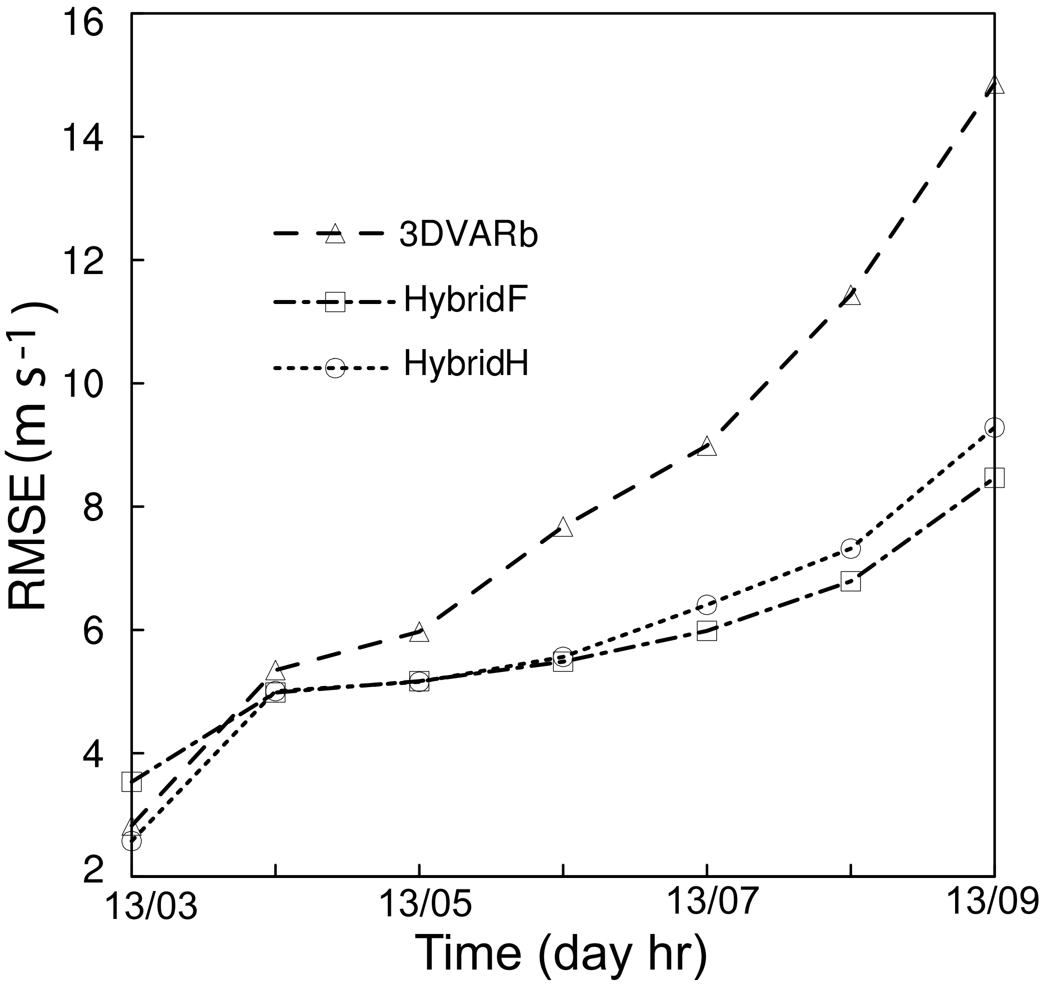

Fig. 13. Deterministic forecast RMSEs of Vr (m s^{-1}) by 3DVARb, HybridF, and HybridH from 0300 to 0900 UTC 13 September 2008.

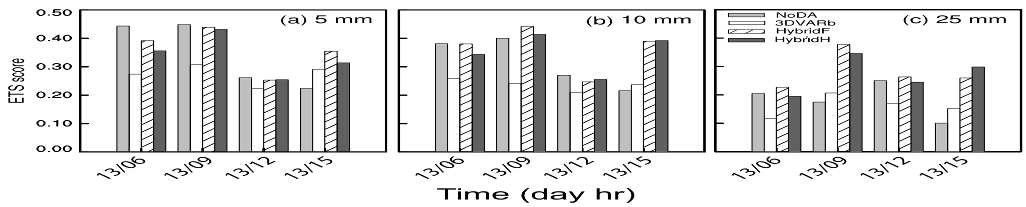

Fig. 14. The equitable threat scores for 3 h accumulated forecast precipitation by NoDA, 3DVARb, HybridF, and HybridH at thresholds (a) 5 mm, (b) 10 mm, and (c) 25 mm, verified against NCEP Stage-IV precipitation analyses valid at 0600, 0900, 1200, and 1500 UTC 13 September 2008.

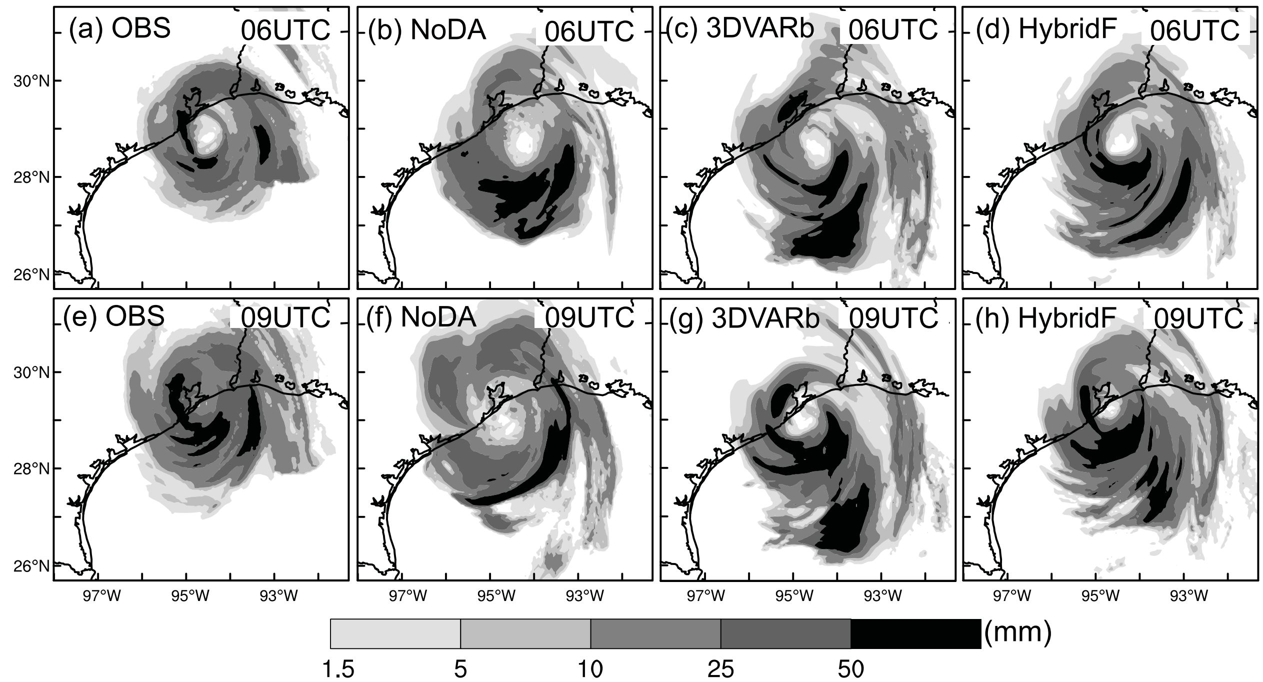

Fig. 15 Three-hour accumulated precipitation (mm) by (1st column) NCEP Stage-IV precipitation analyses, (2nd column) NoDA, (3rd column) 3DVARb, and (4th column) HybridF valid at (top) 0600 and (bottom) 0900 UTC 13 September 2008.